Agricultural and Forest Meteorology 372 (2025) 110704

Contents lists available at ScienceDirect

Agricultural and Forest Meteorology

journal homepage: www.elsevier.com/locate/agrformet

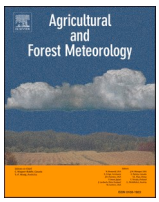

Hysteretic temperature sensitivity in wetland CH_4 emission modeling

Shuo Chen [a], Kunxiaojia Yuan [b,*], Fa Li [c], Qing Zhu [b], Qianlai Zhuang [a,d,*]

[a] Department of Earth, Atmospheric, and Planetary Sciences, Purdue University, West Lafayette, IN, USA
[b] Climate and Ecosystem Sciences Division, Climate Sciences Department, Lawrence Berkeley National Laboratory, Berkeley, CA, USA
[c] Department of Earth System Science, Stanford University, Stanford, CA, USA
[d] Department of Agronomy, Purdue University, West Lafayette, IN, USA

ARTICLE INFO

Keywords:
CH_4 emission
Wetlands
Temperature sensitivity
CH_4 modeling

ABSTRACT

Wetlands account for nearly one-third of total global methane (CH_4) emissions. Recent studies found that the change in substrate availability and microbial activities can cause positive hysteretic temperature sensitivity of wetland CH_4 emissions, which could serve as a critical metric for model evaluation in terms of the timing of peak emissions and their underlying mechanisms. Here, we quantified the CH_4 hysteresis across 25 eddy-covariance sites and compared it with those from 42 models, including 13 biogeochemical models, 22 atmospheric inversion models, and 7 machine learning models. We found 21 out of 25 sites exhibited positive hysteresis of wetland CH_4 emissions in temperate and arctic climate zones. The machine learning models showed a widespread negligible hysteresis pattern. While biogeochemistry and atmospheric inversion models displayed a prevalent positive hysteresis, the atmospheric inversions guided by observed CH_4 concentrations estimated a larger positive hysteresis than that of biogeochemistry models. Overall, most of CH_4 models underestimated temperature hysteresis to different extents compared with the observations at 25 eddy covariance sites. Our research highlights the necessity of constraining the hysteretic temperature sensitivity of wetland CH_4 emissions in process-based biogeochemistry and machine learning models, which will provide more reliable prior information for atmospheric transport and inversion modeling.

1. Introduction

Methane (CH_4) is the second most important greenhouse gas after carbon dioxide (Stocker, 2013) in driving anthropogenic climate change. Wetlands emitted 159 [119–203] Tg CH_4 yr^{-1} globally during 2010–2019, estimated using biogeochemistry models (bottom-up approaches), accounting for nearly one-third of total global CH_4 emissions (Jackson et al., 2024; Saunois et al., 2024). Understanding how wetland CH_4 emissions respond to the environment is important for predicting whether the methane cycle will mitigate or accelerate climate change (Yvon-Durocher et al., 2014).

Wetland CH_4 is produced through anaerobic decomposition of organic matter by methanogens in the anoxia and water-saturated soils (Zhuang et al., 2004). Then, a portion of the CH_4 is oxidized to CO_2 by methanotrophs in aerobic soil layers, while the rest is emitted into the atmosphere through diffusion, ebullition, or plant-mediated transport (Melton et al., 2013). Temperature, substrate availability, and anoxia extent are the most important factors controlling CH_4 production, oxidation, and transportation processes (Saunois et al., 2024). For example, temperature controls microbial activities and CH_4 production rates and the availability of substrates, such as organic material, which serves as the substrate for methanogenesis.

To quantify CH_4 emission, bottom-up (BU) biogeochemical models, top-down (TD) atmospheric transport and inversion models, and machine learning (ML) models were developed. ML models predict CH_4 emissions based on the observed relationship between predictors and CH_4 emissions in the training dataset (Chen et al., 2024). BU models simulate the biogeochemical processes that control CH_4 production, oxidation, and transportation (Zhuang et al., 2004), while the TD models are based on measured atmospheric concentrations to invert their sources and sinks (Bridgham et al., 2013). However, significant discrepancies exist among these models in representing CH_4 processes and their environmental controls (Xu et al., 2016). The simplification of specific biogeochemical processes could lead to uncertainty and bias in the CH_4 emissions simulation.

Hysteresis in CH_4 emissions refers to a phenomenon where the response of CH_4 emissions to a changing environmental factor depends not only on the current state of that factor but also on its past states or

* Correspondence authors.
E-mail addresses: kunxiaojiayuan@lbl.gov (K. Yuan), qzhuang@purdue.edu (Q. Zhuang).

https://doi.org/10.1016/j.agrformet.2025.110704
Received 24 January 2025; Received in revised form 17 May 2025; Accepted 17 June 2025

history (Chang et al., 2020; Moore and Dalva, 1993; Updegraff et al., 1998; Yavitt et al., 1987). Hysteresis between CH_4 and temperature has been reported in previous incubation experiments (Updegraff et al., 1998; Yavitt et al., 1987). Recent studies have further confirmed substantial CH_4-temperature hysteresis across global eddy covariance observations (Chang et al., 2023, 2021). The presence of CH_4-temperature hysteresis suggests CH_4 production does not always respond directly or immediately to the current temperature change. Thus, to improve CH_4 emission simulations, hysteretic temperature sensitivity of wetland CH_4 emissions should be taken into account, but it remains unclear to what extent current CH_4 models can capture the CH_4-temperature hysteresis.

This study quantified the CH_4 hysteresis across 42 CH_4 emission models at 25 eddy-covariance (EC) sites. We then evaluated the ability of the wetland CH_4 models to capture the hysteretic temperature sensitivity of wetland CH_4 emissions. We aim to answer the following questions: (1) What is the hysteretic temperature sensitivity of wetland CH_4 emissions in the Fluxnet-CH_4 observations and model simulations? and (2) How well can models capture the observed hysteresis?

2. Method

2.1. Data

Site-level CH_4 emission data were obtained from FLUXNET-CH_4 and follow the CC-BY-4.0 policy (Delwiche et al., 2021). We selected the seasonal or permanent vegetated wetland but excluded paddy-rice, salt marsh, non-vegetated waterbodies, and drained sites (McNicol et al., 2023). Following the above criterion, 25 eddy covariance sites were finally used in this study (Fig. 1; Table S1). For model comparision, we excluded the sites at the lower latitudes (30°S–30°N) because the sparse data might not be sufficient to support robust conclusions for these regions. Additionally, air temperatures in the lower latitudes are typically above 0 °C year-round, with no freezing and thawing cycles, whereas hysteresis is expected to occur during the freeze-thaw process. Lastly, the sites with data only after 2018 are excluded because the Global Carbon Project-Methane (GCP-CH_4) model output only covers the range from 2000 to 2017. The raw daily CH_4 emission data were converted to the monthly scale by averaging since most model outputs are at monthly resolution. To verify the robustness of the CH_4-temperature hysteresis, the soil temperature data were processed in the same way and used to calculate hysteresis for comparison with air temperature.

Gridded CH_4 emission data were obtained from 13 bottom-up biogeochemical models, 22 top-down models, and 7 machine learning models. The CH_4 emission outputs from bottom-up models and top-down models were obtained from the GCP-CH_4 project (Saunois et al., 2020). The bottom-up models were uniformly forced by CRU-JRA meteorological data, following the GCP-CH_4 protocol (Saunois et al., 2020). The bottom-up CH_4 emission products are at 0.5° spatial resolution and monthly temporal resolution (Saunois et al., 2020). The top-down models were forced by various meteorological data (Table S2). The top-down CH_4 emission products are at 1° spatial resolution and monthly temporal resolution (Saunois et al., 2020). We also included two ML datasets. UpCH_4 was upscaled from eddy covariance measurements from FLUXNET-CH_4 using the random forest model driven by remote sensing vegetation index and meteorological data (McNicol et al., 2023). It is at 0.25° spatial resolution and global spatial coverage. The time period is from 2000 to 2018 at a monthly temporal resolution. Another ML-based dataset was adopted by Chen et al. (2024). It was upscaled from FLUXNET-CH_4 and chamber sites using six ML models, including decision tree (DT), random forest (RF), extreme gradient boosting (XGB), artificial neural network (ANN), Gated Recurrent Units (GRU) and Long Short-Term Memory (LSTM). The models were driven by meteorological data, soil properties, and elevation data. This product is at 0.5° spatial resolution and global spatial coverage. The time period is from 2000 to 2020 at monthly temporal resolution.

To be consistent, gridded air temperature from the ERA5 reanalysis climatic data set (Hersbach et al., 2020) was used to calculate the modeled hysteresis between modeled CH_4 emission and air temperature. ERA5 was originally at 0.25° spatial resolution and monthly temporal resolution and was then resampled to align with the modeled CH_4 emission data. Although the forcing temperature varied from models, the hysteresis patterns are consistent because there are no significant time lags among the different temperature forcing datasets used in the CH_4 models (Fig. S1).

2.2. CH_4 emission hysteresis

We first selected the frost-free season as the period of interest. For observation, the frost-free season was identified as the period when the FLUXNET-CH_4 air temperature is above 0 °C. For model simulation, the frost-free season was identified as the period when the ERA5 air temperature was above 0 °C. The frost-free season was then separated by maximum seasonal temperature (T_{max}) into two segments. The data points observed before T_{max} were identified as the earlier part, while the points after T_{max} were identified as the later parts. Then, we fitted monthly measurements of CH_4 emissions and air temperatures with a quadratic equation Eq. (1) (Chang et al., 2021) for the earlier part ($F_{CH_4,earlier}(T)$) and later part ($F_{CH_4,later}(T)$), exemplified as red and blue lines in Fig. 2c and d:

$$F_{CH_4}(T) = a_{hys}T^2 + \left(\frac{F_{CH_4,\ T_{max}}}{T_{max}} - a_{hys}T_{max}\right) \times T \quad (1)$$

where $F_{CH_4}(T)$ represents CH_4 emission, T represents monthly mean air temperature, T_{max} represents maximum seasonal air temperature, $F_{CH_4,\ T_{max}}$ represents CH_4 emission measured at maximum seasonal air temperature and a_{hys} represents the hysteresis parameter that determines the quadratic function.

To quantify the magnitude of CH_4 emission hysteresis, we calculated the normalized area (H_A) enclosed by the earlier period model ($F_{CH_4,earlier}(T)$) and the later period model ($F_{CH_4,later}(T)$):

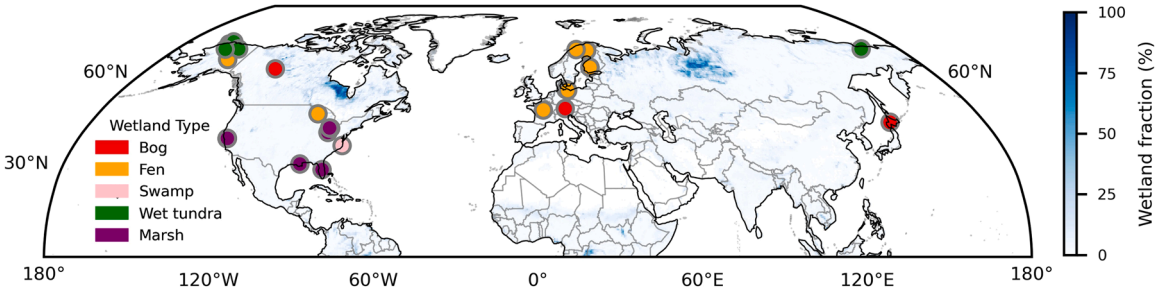

Fig. 1. Location and wetland type of 25 EC sites. Symbol colors represent the wetland type. The wetland fraction was derived from the WAD2AM (Zhang et al., 2021) wetland distribution map.

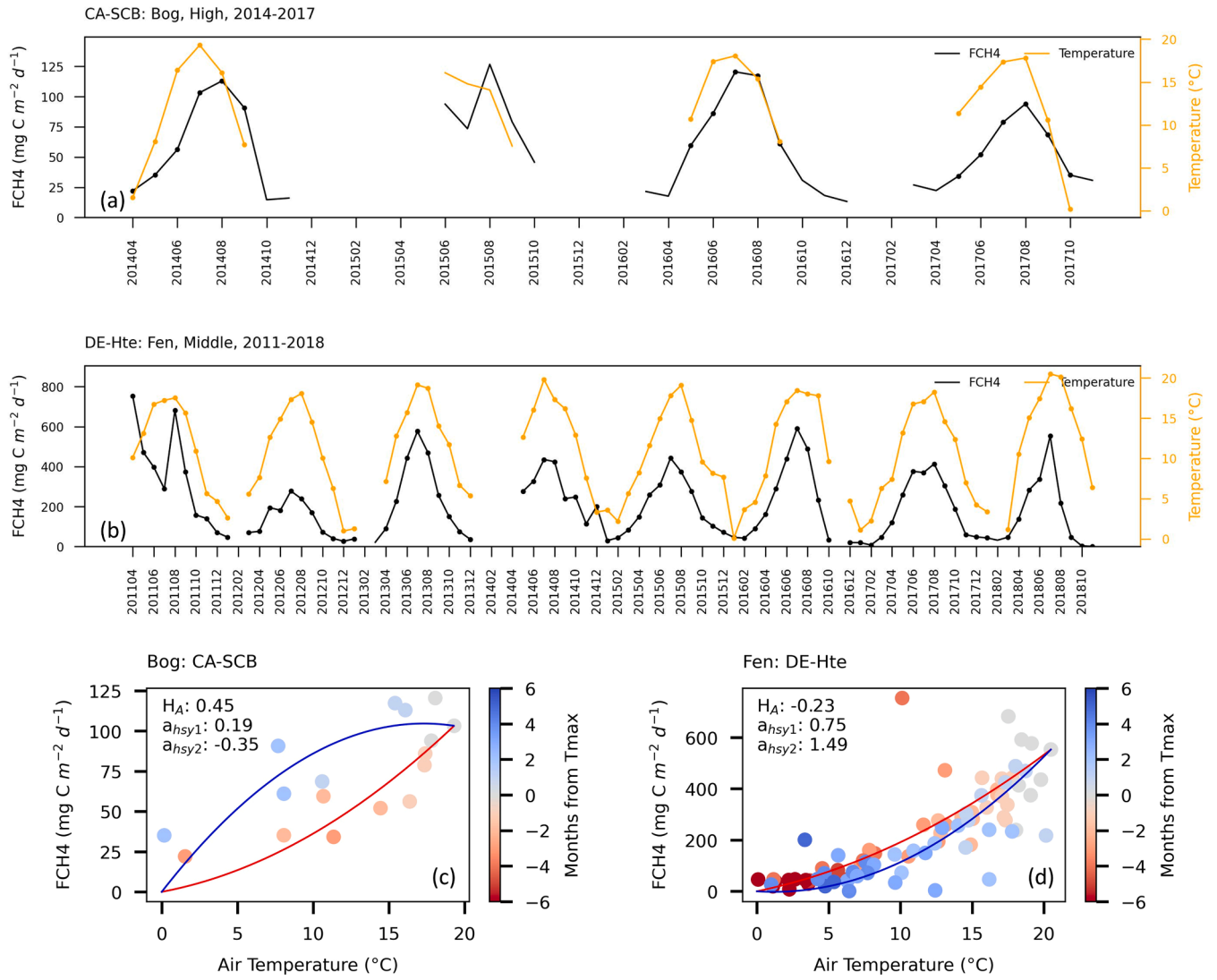

Fig. 2. Observed temperature sensitivity and time series of wetland CH_4 emissions at sites CA-SCB and DE-Hte. The data points used for (c) and (d) are marked with dots in (a) and (b).

$$H_A = \frac{\int_0^{T_{max}} \left(F_{CH_4,later}(T) - F_{CH_4,earlier}(T)\right) dT}{max\left(abs\left(F_{CH_4,earlier}(T), F_{CH_4,later}(T)\right)\right) T_{max}} \quad (2)$$

2.3. Model comparison

To evaluate the ability of the model to estimate the CH_4 hysteresis, we first extracted the modeled CH_4 emissions values of the grid cells where the eddy-covariance sites are located. Then, we followed the same approach (Eqs. 1 and 2) to calculate modeled hysteresis. Finally, the mean bias errors (MBE) between modeled and observed hysteresis were calculated as follows:

$$MBE = \frac{1}{n}\sum_{i}^{n}\left(\widehat{H_{Ai}} - H_{Ai}\right) \quad (3)$$

The symbols used in Eq. (3) denote modeled hysteresis ($\widehat{H_{Ai}}$), observed hysteresis (H_{Ai}), and number of sites (n).

3. Results

3.1. Seasonal CH_4 emission hysteresis at EC sites

Fig. 2 shows examples of two EC sites with different patterns of CH_4 emission hysteresis. The dynamics of CH_4 emissions usually followed the change in air temperature and showed an exponential relationship with air temperature. However, for those sites with positive hysteresis, the peaks of CH_4 emissions tended to occur after the maximum temperature (Fig. 2a). For example, at site CA-SCB, its maximum air temperature occurred in July, while the peak CH_4 emissions occurred in August 2014 (Fig. 2a). Furthermore, the time-dependent CH_4-temperature relationship varied from earlier to later parts of the thawed season. At site CA-SCB, the area enclosed by the later period model ($F_{CH_4,later}(T)$) was larger than the earlier period model ($F_{CH_4,earlier}(T)$), with a positive a_{hys} in the earlier part and a negative a_{hys} in the later part (Fig. 3a). It indicated that CH_4 emissions are higher in the later frost-free season at the same air temperature (Fig. 2c), known as a positive seasonal hysteresis.

Positive seasonal CH_4-temperature hysteresis was observed at most sites recorded in the FLUXNET-CH_4 database (Fig. 3b). Negative temperature hysteresis is only observed among sites DE-Hte, DE-Zrk, US-Orv, and US-Tw5 (Fig. 3b). The CH_4 emissions of these sites could be controlled by other variables (e.g., water table depth or salinity) rather than temperature, in which case hysteresis would not apply (Chamberlain et al., 2020; Chang et al., 2021).

Hysteresis between CH_4 emissions and soil temperature is also observed at most eddy covariance sites (Table S3). Only 3 (out of 25) sites exhibit different signs of hysteresis with air temperature, namely

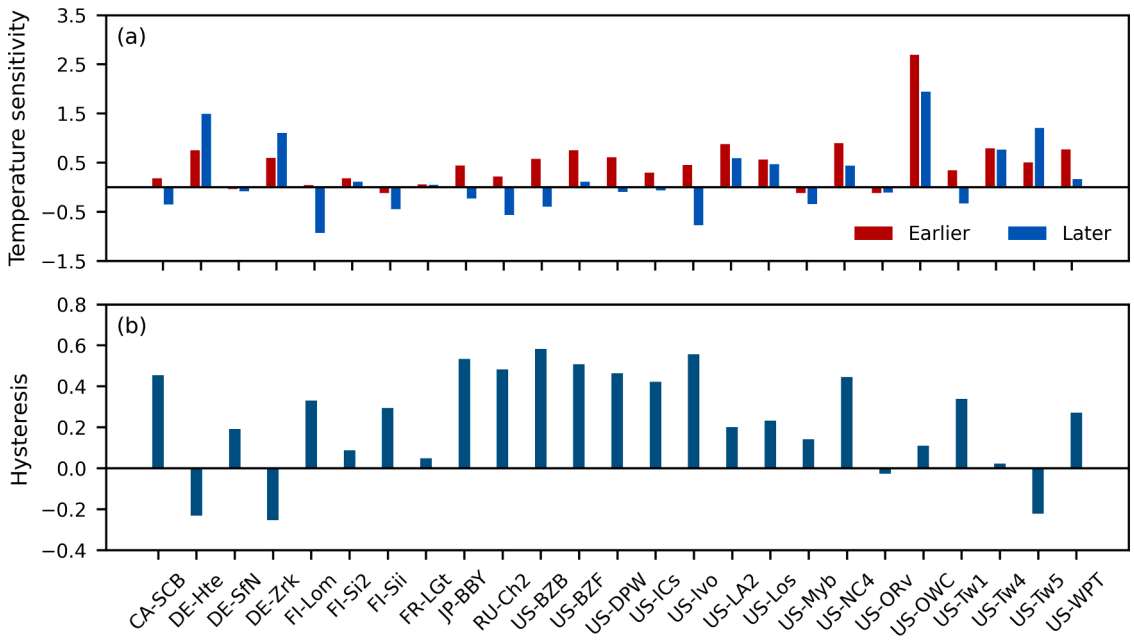

Fig. 3. Observed (a) temperature sensitivity (a_{hys}) and (b) CH_4-temperature hysteresis at EC sites.

DE-SfN, US-BZF, and US-Los (Table S3). The rest of the sites show the same signs of hysteresis except sites US-DPW and US-LA2, which don't provide soil temperature measurements. Therefore, the observed hysteresis is prevalent across at least 20 sites, regardless of whether air temperature or soil temperature is used. We focus on air temperature rather than soil temperature in the following sections, as air temperature data is generally available and continuous at observational sites.

3.2. Seasonal CH_4 emission hysteresis among CH_4 models

ML, BU, and TD models had varying abilities to capture the observed hysteresis (Fig. 4). Taking site CA-SCB as an example, ML models simulated negative hysteresis (−0.12) (Fig. 4a), which was the opposite of the observed positive hysteresis (0.45). BU models (0.23) and TD models (0.37) captured the positive hysteresis with underestimation (Fig. 4b–c). As for site DE-Hte, ML, BU, and TD models can simulate the observed negative hysteresis (−0.23), and BU models gave a closer

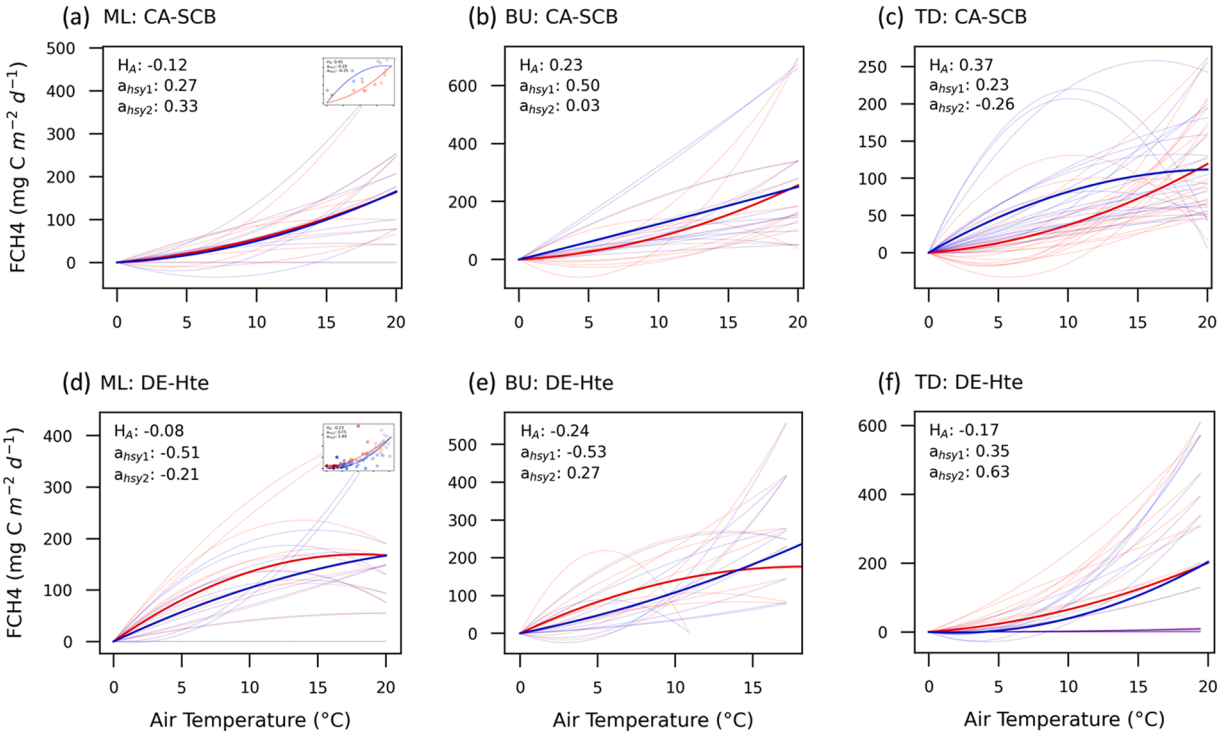

Fig. 4. ML (a,d), bottom-up (b,e), and top-down (c,f) modeled temperature sensitivity of wetland CH_4 emissions at CA-SCB (upper panel) and DE-Hte (lower panel). The light-colored lines represent the quadratic equation for the earlier part ($F_{CH_4,earlier}(T)$) and the later part ($F_{CH_4,later}(T)$), calculated from individual models, while the dark-colored lines represent the model average.

estimation (−0.24) (Fig. 4d–f). It should also be noted that there is a large uncertainty in the hysteresis estimates even within the same category of the models (Fig. 4).

Overall, ML models displayed negative hysteresis in the Russian Far East and Western China while positive hysteresis in the rest (Fig. 5a). BU models displayed mainly positive hysteresis for areas north of 45°N latitude while mainly negative hysteresis in the rest (Fig. 5b). TD models displayed a similar spatial pattern as BU models but with a larger magnitude (Fig. 5c).

3.3. Model comparison

Observed CH_4 emissions had higher positive hysteresis in the high-latitude regions (>60°N) than in the middle latitudes (30–60°N) (Fig. 6a). The intra-seasonal changes in emergent CH_4-T_{air} dependence vary substantially among wetland types (Fig. 6b). Bog and wet tundra sites had higher positive hysteresis than fen and marsh, especially all wet tundra sites have positive hysteresis (Fig. 6b). These patterns were captured by modeled CH_4 emissions, but the magnitude of hysteresis was underestimated (Fig. 6).

More than half of the models underestimated CH_4-temperature hysteresis (Fig. 7). For bog, all ML models, 11 of 13 BU models, and 20 of 22 TD models underestimate the hysteresis of the bog sites (Fig. 7). For fen, 6 of 7 ML models, 9 of 13 BU models, and 12 of 22 TD models slightly underestimated the hysteresis (Fig. 7). For marsh, 6 of 7 ML models, 6 of 13 BU models, and 10 of 22 TD models underestimated the hysteresis (Fig. 7). For wet tundra, all ML models, 7 of 13 BU models, and 7 of 22 TD models underestimated the CH_4-temperature hysteresis (Fig. 7).

4. Discussion

4.1. Factors modulating CH_4-temperature hysteresis

The magnitude and variability of CH_4 emissions are strongly influenced by various environmental conditions, physiological processes, and microbial dynamics through the CH_4 production, oxidation, and transport processes. Various factors can contribute to hysteresis, and one widely accepted explanation is microbial substrate-mediated CH_4 production supported by previous incubation experiments (Updegraff et al., 1998, 1995; Valentine et al., 1994; Yavitt et al., 1987) and model simulations (Chadburn et al., 2020; Chang et al., 2020; Tang and Riley, 2015). The experiments reported by Yavitt et al. (1987) revealed that the thermal history of the substrate modulated the response of CH_4 emissions to temperature change as soil samples collected in different seasons exhibited significantly different CH_4 emission rates, even under isothermal incubation conditions. Furthermore, in the experiments reported by Updegraff et al. (1998), soil samples were collected from the same location at different times during the season and incubated under controlled environmental conditions (e.g., moisture, pH, and oxygen). They found that CH_4 production rates were higher, and hysteresis was most pronounced during the early post-thaw season when more labile substrates were available (Updegraff et al., 1998). It suggested the hysteresis effect is closely linked to the seasonal differences in microbial communities and substrate availability (Updegraff et al., 1998), as the primary role of temperature is regulating substrate supply through fermentation rates in CH_4 production (Updegraff et al., 1995; Valentine et al., 1994).

Moreover, the model simulations also suggested that microbial process and substrate availability mediated the CH_4-temperature hysteresis (Chadburn et al., 2020; Chang et al., 2020; Grant, 1998; Tang and Riley, 2015). The *ecosys* model is one of the few existing models that comprehensively represent key CH_4 processes and mechanisms, including microbial activity and two primary substrate pathways: acetate and single-carbon compounds (Grant, 1998; Xu et al., 2016). The *ecosys* simulation showed that the CH_4-temperature hysteresis was mainly dominated by CH_4 production rather than oxidation, as the modeled CH_4 production is the highest while the CH_4 oxidation rate is relatively low during the thawed season when the hysteresis is the most pronounced (Chang et al., 2020). Also, the hysteresis might be closely linked to substrate availability because the modeled substrate availability also peaks after the maximum temperature, exhibiting a similar pattern of CH_4 production (Chang et al., 2020). Moreover, Chadburn et al. (2020) incorporated microbial modules into the standard JULES model. The JULES-microbe model reduced the root mean squared error of modeled CH_4 emissions by 10–25 % and successfully reproduced the observed CH_4-temperature hysteresis (Chadburn et al., 2020). These lines of evidence suggest that the inadequate inclusion of substrate availability and microbial dynamics might be the main cause of the underrepresentation of the hysteresis effect in the CH_4 models.

On the other hand, some other factors could also modulate the hysteretic effect between temperature and CH_4 emissions, such as water

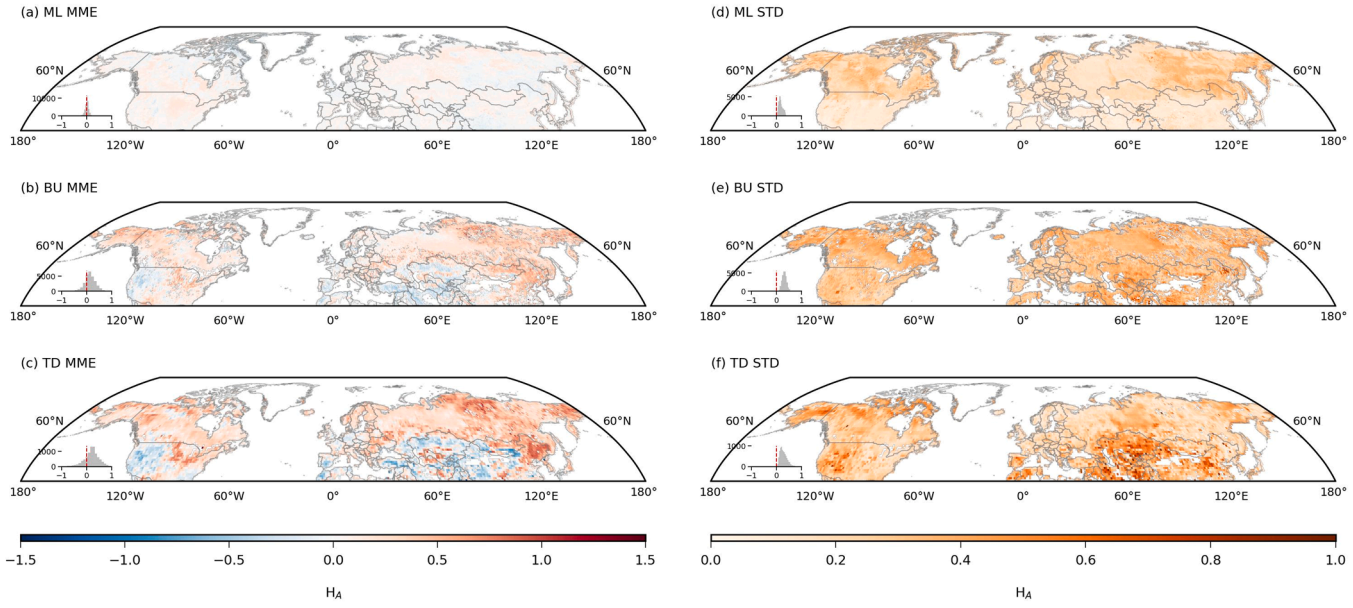

Fig. 5. Spatial distribution of multi-model ensemble mean (a,b,c) and standard deviation (d,e,f) of CH_4 emission hysteresis.

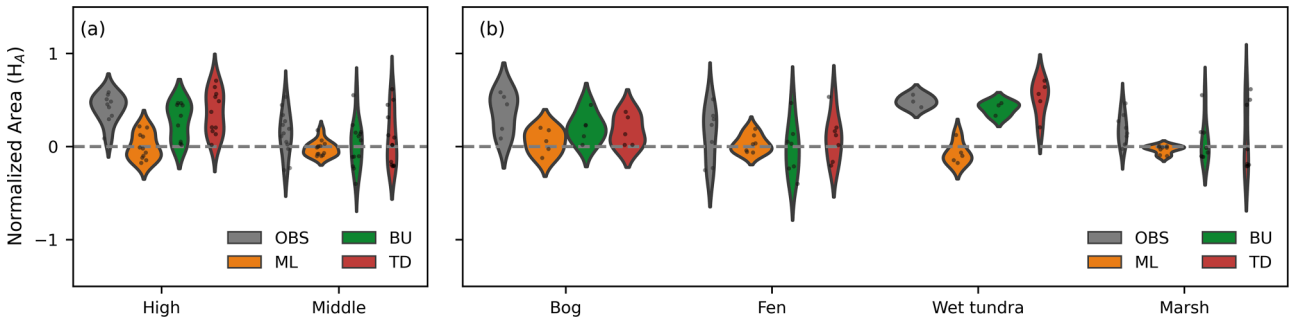

Fig. 6. Violin plots of hysteresis at sites. In the x-axis, "high" represents high latitudes, and "middle" represents middle latitudes regions.

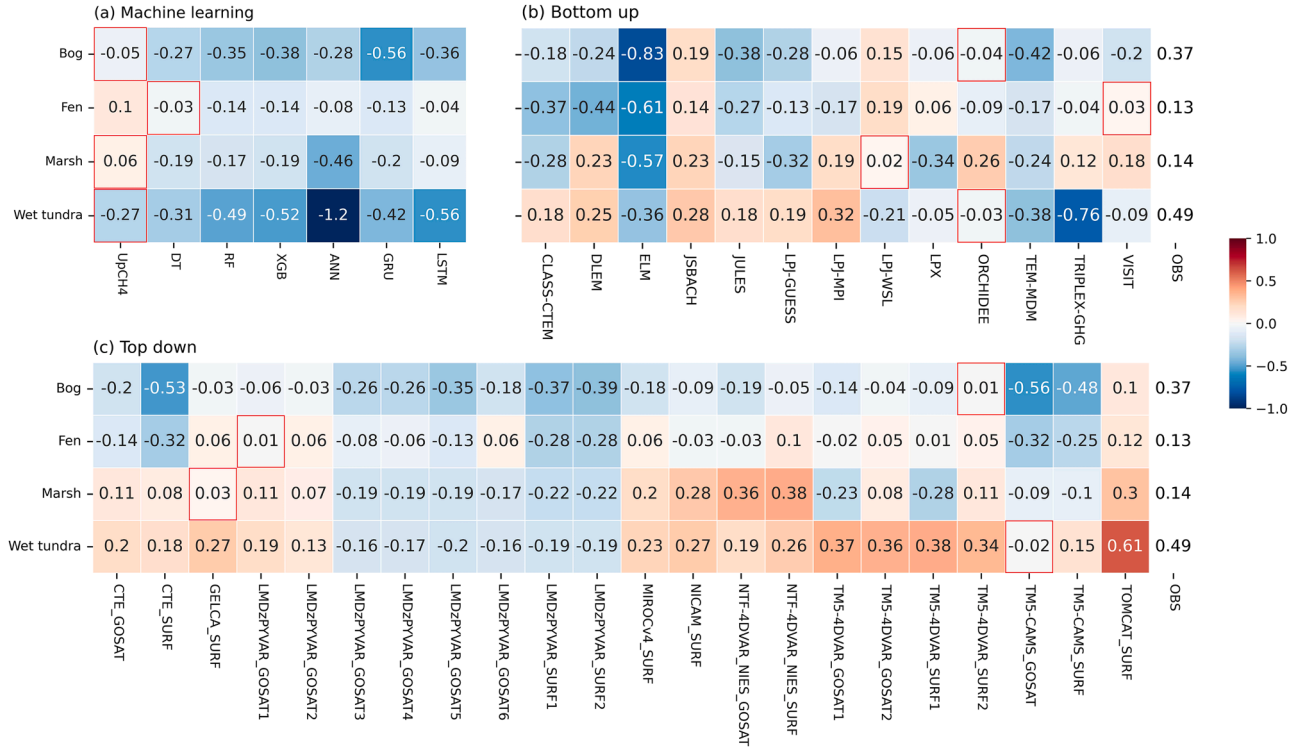

Fig. 7. Mean bias errors between modeled and observed hysteresis. The model with the smallest absolute mean bias error of each ecosystem is highlighted by the red rectangle. The average observed hysteresis is presented in the last column.

table depth (Brown et al., 2014; Moore and Dalva, 1993), gross primary productivity (Mitra et al., 2020; Rinne et al., 2018) and vegetation composition (Olefeldt et al., 2013; Pangala et al., 2017). For example, previous research reported hysteresis between water table depth and CH_4 emissions due to the release of CH_4 from pore spaces and bubbles (Moore and Dalva, 1993). Also, the time lag in the conversion from gross primary production to substrate could also raise hysteresis between gross primary production and CH_4 emissions (Rinne et al., 2018). However, the available observation is insufficient to support comprehensive and mechanistic explanations for the CH_4-temperature hysteresis. In the future, additional incubation experiments and field observations on the above factors are necessary to incorporate these potential phenomena and control mechanisms into mechanistic explanations, thereby improving model calibration and parameterization.

4.2. Current model representation of hysteretic temperature sensitivity of wetland CH_4 emissions

ML models leverage the given environmental predictors to estimate CH_4 emissions based on observed patterns and correlations. $UpCH_4$ and Chen2024 products used similar predictors. Specifically, $UpCH_4$ was driven by air temperature, precipitation, enhanced vegetation index, and vegetation canopy height (McNicol et al., 2023). The Chen2024 products were driven by air temperature, precipitation, surface downward solar radiation, relative humidity, soil properties, elevation, and wetland type (Chen et al., 2024). $UpCH_4$ relatively outperforms the Chen2024 product likely because $UpCH_4$ additionally incorporates time-lagged EVI and air temperature besides the common predictors used by both products. In $UpCH_4$, EVI might serve as a proxy for substrate availability, and time-lagged temperature might capture the effects of thermal history, which together help capture the hysteretic temperature sensitivity of wetland CH_4 emissions.

The BU biogeochemical models were developed for a variety of purposes and with a tradeoff between having an explicit representation of mechanisms and appropriate model complexities (Evans et al., 2013; Tang and Zhuang, 2009). Most of the BU models represent the relationship between CH_4 production and substrate availability using a function that links CH_4 production with heterotrophic respiration or soil organic matter content and is constrained by multiple environmental factors (Table S4). For example, the LPJ family models defined CH_4

production as heterotrophic respiration multiplied by response functions related to temperature and water content (Hodson et al., 2011; Spahni et al., 2011; Wania et al., 2010, 2009). The second group of models represents the substrate pool by dissolved organic carbon or soil organic carbon (Table S4). For example, DLEM defined CH_4 production as dissolved organic carbon multiplied by the response functions of temperature, pH, and water content (Tian et al., 2015, 2010). In either case, the CH_4 production is usually dependent on the temperature at the given time point (e.g. $P_{CH_4} = f(T)_t + \varepsilon$) using a linear function or Q10 function (Table S4). However, previous research suggested that substrate availability at any given point in time would reflect the both previous and current temperature regime (Moore and Dalva, 1993; Updegraff et al., 1998). Thus, the history of change in temperature ($\int_{\tau=0}^{t} g(T_\tau)d\tau$) should be considered in the temperature response function (e.g. $P_{CH_4} = f(T)_t + \int_{\tau=0}^{t} g(T_\tau)d\tau + \varepsilon$). Additionally, the microbial modules have not been included in the examined models (Xu et al., 2016).

TD models underestimate hysteresis less than the BU models and ML models could be because they used satellite or surface CH_4 observations to constrain CH_4 emissions besides prior estimates from BU models. More accurate BU and ML estimates are an important prerequisite to further improve the capability of TD models in simulating temperature hysteresis since TD models strongly rely on the prior BU/ML emission estimates in their inversion framework (Houweling et al., 2017; Inoue et al., 2016; Maasakkers et al., 2021).

4.3. Implication for modeling wetland CH_4 emissions

The inadequate inclusion of the hysteresis effect on CH_4 emission results in a 11.6 % overestimation of CH_4 emissions in the earlier period and an 4.2 % underestimation in the later period at middle latitudes (Fig. S2a). The bias is more pronounced at high latitudes, with a 40 % overestimation in the earlier season and a 14.1 % underestimation in the later season (Fig. S2b). These discrepancies could result in uncertainty in our understanding and projections of climate change impacts since CH_4 emissions are a critical component of the global carbon budget and climate feedback mechanisms (Saunois et al., 2017, pp. 2000–2012; Van Vuuren et al., 2011). Additionally, without accounting for the hysteresis, CH_4 models could fail to reproduce seasonal variation patterns of CH_4 emissions. For example, modeled CH_4 emissions might peak earlier than the actual time point, limiting the ability to identify the actual hotspots and seasonal peaks.

Advanced time series models (e.g., recurrent neural networks or transformers) are promising to improve the ability of the ML model to simulate hysteretic temperature effects. They are designed to learn short- and long-term dependencies in time-series data and remember information for prolonged periods of time (Hochreiter and Schmidhuber, 1997). They should be able to learn the change of temperature sensitivity when methanogen biomass and substrate are changing over time. A current attempt has been successfully implemented through a causality-guided ML model and demonstrated at 30 wetland sites (Yuan et al., 2022). Besides the improvement of the model structure, it is also important to constrain the black-box ML models with biogeochemical knowledge of methane dynamics (Liu et al., 2024, 2022). For example, Liu et al. (2022) developed a knowledge-guided machine learning framework by constraining recurrent neural networks by incorporating bio-geophysical and chemical domain knowledge from the *ecosys* model.

For BU models, using the modified Boltzmann–Arrhenius function to represent temperature may be a solution to capture the hysteretic responses of CH_4 emissions since it considers the exponential relationship between metabolic rate and temperature rather than a static temperature function (Chang et al., 2020; Yvon-Durocher et al., 2014). For example, *ecosys* can simulate the declining Q10 of heterotrophic respiration with increasing soil temperature using a modified Arrhenius function that includes the terms for low- and high-temperature inactivation (Grant, 2015). Current efforts are also devoted to incorporating microbial dynamics into BU models (Oh et al., 2020; Wang et al., 2019; Xu et al., 2015). The improvement of ML models and BU models will further help improve TD models by providing more reliable prior information.

5. Conclusion

This research quantified the CH_4 temperature hysteresis metric across 25 eddy-covariance sites and compared it against the estimates from 42 CH_4 emission models. We found that 21 out of 25 sites exhibited positive hysteresis of wetland CH_4 emissions covering both temperate and arctic climate zones. ML models displayed a widespread small magnitude of hysteresis. BU and TD models displayed prevalent positive hysteresis, and TD models estimated a larger positive hysteresis than that of BU models. However, the modeled CH_4 emissions overall underestimated temperature hysteresis compared with the observations among 25 eddy covariance sites. Our research highlights the necessity of constraining the hysteretic temperature sensitivity of CH_4 emissions by including substrate availability and microbial activity in BU models as well as considering time-lagged controls and physical constraints in ML models. They will further help improve TD models by providing more reliable prior information.

CRediT authorship contribution statement

Shuo Chen: Writing – review & editing, Writing – original draft, Visualization, Software, Methodology, Formal analysis, Data curation, Conceptualization. **Kunxiaojia Yuan:** Writing – review & editing, Supervision, Resources, Methodology, Data curation, Conceptualization. **Fa Li:** Writing – review & editing, Methodology, Conceptualization. **Qing Zhu:** Writing – review & editing, Resources, Methodology, Conceptualization. **Qianlai Zhuang:** Writing – review & editing, Supervision, Resources, Funding acquisition.

Declaration of competing interest

The authors declare that they have no known competing financial interests or personal relationships that could have appeared to influence the work reported in this paper.

Acknowledgments

This study was supported through a project funded to Q.Z. by NASA (NNX17AK20G). Lawrence Berkeley National Laboratory (LBNL) is managed by the University of California for the U.S. Department of Energy under contract DE-AC02-05CH11231. K.Y. is supported by an Early Career Development Grant (ECDG), which was sponsored by the Earth and Environmental Sciences Area of Lawrence Berkeley National Laboratory. We thank the research teams contributing to the FLUXNET-CH_4 (Delwiche et al., 2021) and GCP-CH_4 (Saunois, et al., 2020) Synthesis Activities.

Supplementary materials

Supplementary material associated with this article can be found, in the online version, at doi:10.1016/j.agrformet.2025.110704.

Data availability

Data will be made available on request.

References

Bridgham, S.D., Cadillo-Quiroz, H., Keller, J.K., Zhuang, Q., 2013. Methane emissions from wetlands: biogeochemical, microbial, and modeling perspectives from local to global scales. Glob Chang. Biol. 19, 1325–1346. https://doi.org/10.1111/gcb.12131.

Brown, M.G., Humphreys, E.R., Moore, T.R., Roulet, N.T., Lafleur, P.M., 2014. Evidence for a nonmonotonic relationship between ecosystem-scale peatland methane emissions and water table depth. J. Geophys. Res.: Biogeosci. 119, 826–835. https://doi.org/10.1002/2013JG002576.

Chadburn, S.E., Aalto, T., Aurela, M., Baldocchi, D., Biasi, C., Boike, J., Burke, E.J., Comyn-Platt, E., Dolman, A.J., Duran-Rojas, C., Fan, Y., Friborg, T., Gao, Y., Gedney, N., Göckede, M., Hayman, G.D., Holl, D., Hugelius, G., Kutzbach, L., Lee, H., Lohila, A., Parmentier, F.-J.W., Sachs, T., Shurpali, N.J., Westermann, S., 2020. Modeled microbial dynamics explain the apparent temperature sensitivity of wetland methane emissions. Global Biogeochem. Cycles 34, e2020GB006678. https://doi.org/10.1029/2020GB006678.

Chamberlain, S.D., Hemes, K.S., Eichelmann, E., Szutu, D.J., Verfaillie, J.G., Baldocchi, D.D., 2020. Effect of drought-induced salinization on wetland methane emissions, gross ecosystem productivity, and their interactions. Ecosystems 23, 675–688. https://doi.org/10.1007/s10021-019-00430-5.

Chang, K.-Y., Riley, W.J., Collier, N., McNicol, G., Fluet-Chouinard, E., Knox, S.H., Delwiche, K.B., Jackson, R.B., Poulter, B., Saunois, M., Chandra, N., Gedney, N., Ishizawa, M., Ito, A., Joos, F., Kleinen, T., Maggi, F., McNorton, J., Melton, J.R., Miller, P., Niwa, Y., Pasut, C., Patra, P.K., Peng, C., Peng, S., Segers, A., Tian, H., Tsuruta, A., Yao, Y., Yin, Y., Zhang, W., Zhang, Z., Zhu, Qing, Zhu, Qiuan, Zhuang, Q., 2023. Observational constraints reduce model spread but not uncertainty in global wetland methane emission estimates. Glob Chang. Biol. 29, 4298–4312. https://doi.org/10.1111/gcb.16755.

Chang, K.-Y., Riley, W.J., Crill, P.M., Grant, R.F., Saleska, S.R., 2020. Hysteretic temperature sensitivity of wetland CH<sub>4</sub&gt. fluxes explained by substrate availability and microbial activity. https://doi.org/10.5194/bg-2020-177.

Chang, K.-Y., Riley, W.J., Knox, S.H., Jackson, R.B., McNicol, G., Poulter, B., Aurela, M., Baldocchi, D., Bansal, S., Bohrer, G., Campbell, D.I., Cescatti, A., Chu, H., Delwiche, K.B., Desai, A.R., Euskirchen, E., Friborg, T., Goeckede, M., Helbig, M., Hemes, K.S., Hirano, T., Iwata, H., Kang, M., Keenan, T., Krauss, K.W., Lohila, A., Mammarella, I., Mitra, B., Miyata, A., Nilsson, M.B., Noormets, A., Oechel, W.C., Papale, D., Peichl, M., Reba, M.L., Rinne, J., Runkle, B.R.K., Ryu, Y., Sachs, T., Schäfer, K.V.R., Schmid, H.P., Shurpali, N., Sonnentag, O., Tang, A.C.I., Torn, M.S., Trotta, C., Tuittila, E.-S., Ueyama, M., Vargas, R., Vesala, T., Windham-Myers, L., Zhang, Z., Zona, D., 2021. Substantial hysteresis in emergent temperature sensitivity of global wetland CH4 emissions. Nat. Commun. 12, 2266. https://doi.org/10.1038/s41467-021-22452-1.

Chen, S., Liu, L., Yuchi, M., Zhuang, Q., Shurpali, N.J., 2024. Quantifying global wetland methane emissions with in situ methane flux data and machine learning approaches. Earth's Future 12. https://doi.org/10.1029/2023EF004330.

Delwiche, K.B., Knox, S.H., Malhotra, A., Fluet-Chouinard, E., McNicol, G., Feron, S., Ouyang, Z., Papale, D., Trotta, C., Canfora, E., Cheah, Y.-W., Christianson, D., Alberto, M.C.R., Alekseychik, P., Aurela, M., Baldocchi, D., Bansal, S., Billesbach, D. P., Bohrer, G., Bracho, R., Buchmann, N., Campbell, D.I., Celis, G., Chen, J., Chen, W., Chu, H., Dalmagro, H.J., Dengel, S., Desai, A.R., Detto, M., Dolman, H., Eichelmann, E., Euskirchen, E., Famulari, D., Fuchs, K., Goeckede, M., Gogo, S., Gondwe, M.J., Goodrich, J.P., Gottschalk, P., Graham, S.L., Heimann, M., Helbig, M., Helfter, C., Hemes, K.S., Hirano, T., Hollinger, D., Hörtnagl, L., Iwata, H., Jacotot, A., Jurasinski, G., Kang, M., Kasak, K., King, J., Klatt, J., Koebsch, F., Krauss, K.W., Lai, D.Y.F., Lohila, A., Mammarella, I., Belelli Marchesini, L., Manca, G., Matthes, J. H., Maximov, T., Merbold, L., Mitra, B., Morin, T.H., Nemitz, E., Nilsson, M.B., Niu, S., Oechel, W.C., Oikawa, P.Y., Ono, K., Peichl, M., Peltola, O., Reba, M.L., Richardson, A.D., Riley, W., Runkle, B.R.K., Ryu, Y., Sachs, T., Sakabe, A., Sanchez, C.R., Schuur, E.A., Schäfer, K.V.R., Sonnentag, O., Sparks, J.P., Stuart-Haëntjens, E., Sturtevant, C., Sullivan, R.C., Szutu, D.J., Thom, J.E., Torn, M.S., Tuittila, E.-S., Turner, J., Ueyama, M., Valach, A.C., Vargas, R., Varlagin, A., Vazquez-Lule, A., Verfaillie, J.G., Vesala, T., Vourlitis, G.L., Ward, E.J., Wille, C., Wohlfahrt, G., Wong, G.X., Zhang, Z., Zona, D., Windham-Myers, L., Poulter, B., Jackson, R.B., 2021. FLUXNET-CH_4: a global, multi-ecosystem dataset and analysis of methane seasonality from freshwater wetlands. Earth System Sci. Data 13, 3607–3689. https://doi.org/10.5194/essd-13-3607-2021.

Evans, M.R., Grimm, V., Johst, K., Knuuttila, T., de Langhe, R., Lessells, C.M., Merz, M., O'Malley, M.A., Orzack, S.H., Weisberg, M., Wilkinson, D.J., Wolkenhauer, O., Benton, T.G., 2013. Do simple models lead to generality in ecology? Trends Ecol. Evol. (Amst.) 28, 578–583. https://doi.org/10.1016/j.tree.2013.05.022.

Grant, R.F., 2015. Ecosystem CO2 and CH4 exchange in a mixed tundra and a fen within a hydrologically diverse Arctic landscape: 2. Modeled impacts of climate change. J. Geophysical. Res.: Biogeosci. 120, 1388–1406. https://doi.org/10.1002/2014JG002889.

Grant, R.F., 1998. Simulation of methanogenesis in the mathematical model *ecosys*. Soil Biol. Biochem. 30, 883–896. https://doi.org/10.1016/S0038-0717(97)00218-6.

Hersbach, H., Bell, B., Berrisford, P., Hirahara, S., Horányi, A., Muñoz-Sabater, J., Nicolas, J., Peubey, C., Radu, R., Schepers, D., Simmons, A., Soci, C., Abdalla, S., Abellan, X., Balsamo, G., Bechtold, P., Biavati, G., Bidlot, J., Bonavita, M., De Chiara, G., Dahlgren, P., Dee, D., Diamantakis, M., Dragani, R., Flemming, J., Forbes, R., Fuentes, M., Geer, A., Haimberger, L., Healy, S., Hogan, R.J., Hólm, E., Janisková, M., Keeley, S., Laloyaux, P., Lopez, P., Lupu, C., Radnoti, G., De Rosnay, P., Rozum, I., Vamborg, F., Villaume, S., Thépaut, J., 2020. The ERA5 global reanalysis. Quart J Royal Meteoro Soc 146, 1999–2049. https://doi.org/10.1002/qj.3803.

Hochreiter, S., Schmidhuber, J., 1997. Long short-term memory. Neural Comput. 9, 1735–1780. https://doi.org/10.1162/neco.1997.9.8.1735.

Hodson, E.L., Poulter, B., Zimmermann, N.E., Prigent, C., Kaplan, J.O., 2011. The El Niño–Southern Oscillation and wetland methane interannual variability. Geophys. Res. Lett. 38. https://doi.org/10.1029/2011GL046861.

Houweling, S., Bergamaschi, P., Chevallier, F., Heimann, M., Kaminski, T., Krol, M., Michalak, A.M., Patra, P., 2017. Global inverse modeling of CH_4 sources and sinks: an overview of methods. Atmos. Chem. Phys. 17, 235–256. https://doi.org/10.5194/acp-17-235-2017.

Inoue, M., Morino, I., Uchino, O., Nakatsuru, T., Yoshida, Y., Yokota, T., Wunch, D., Wennberg, P.O., Roehl, C.M., Griffith, D.W.T., Velazco, V.A., Deutscher, N.M., Warneke, T., Notholt, J., Robinson, J., Sherlock, V., Hase, F., Blumenstock, T., Rettinger, M., Sussmann, R., Kyrö, E., Kivi, R., Shiomi, K., Kawakami, S., De Mazière, M., Arnold, S.G., Feist, D.G., Barrow, E.A., Barney, J., Dubey, M., Schneider, M., Iraci, L.T., Podolske, J.R., Hillyard, P.W., Machida, T., Sawa, Y., Tsuboi, K., Matsueda, H., Sweeney, C., Tans, P.P., Andrews, A.E., Biraud, S.C., Fukuyama, Y., Pittman, J.V., Kort, E.A., Tanaka, T., 2016. Bias corrections of GOSAT SWIR XCO_2 and XCH_4 with TCCON data and their evaluation using aircraft measurement data. Atmos. Meas. Tech. 9, 3491–3512. https://doi.org/10.5194/amt-9-3491-2016.

Jackson, R.B., Saunois, M., Martinez, A., Canadell, J.G., Yu, X., Li, M., Poulter, B., Raymond, P.A., Regnier, P., Ciais, P., Davis, S.J., Patra, P.K., 2024. Human activities now fuel two-thirds of global methane emissions. Environ. Res. Lett. 19, 101002. https://doi.org/10.1088/1748-9326/ad6463.

Liu, L., Xu, S., Tang, J., Guan, K., Griffis, T.J., Erickson, M.D., Frie, A.L., Jia, X., Kim, T., Miller, L.T., Peng, B., Wu, S., Yang, Y., Zhou, W., Kumar, V., Jin, Z., 2022. KGML-ag: a modeling framework of knowledge-guided machine learning to simulate agroecosystems: a case study of estimating N₂O emission using data from mesocosm experiments. Geosci. Model Dev. 15, 2839–2858. https://doi.org/10.5194/gmd-15-2839-2022.

Liu, L., Zhou, W., Guan, K., Peng, B., Xu, S., Tang, J., Zhu, Q., Till, J., Jia, X., Jiang, C., Wang, S., Qin, Z., Kong, H., Grant, R., Mezbahuddin, S., Kumar, V., Jin, Z., 2024. Knowledge-guided machine learning can improve carbon cycle quantification in agroecosystems. Nat. Commun. 15, 357. https://doi.org/10.1038/s41467-023-43860-5.

Maasakkers, J.D., Jacob, D.J., Sulprizio, M.P., Scarpelli, T.R., Nesser, H., Sheng, J., Zhang, Y., Lu, X., Bloom, A.A., Bowman, K.W., Worden, J.R., Parker, R.J., 2021. 2010-2015 North American methane emissions, sectoral contributions, and trends: a high-resolution inversion of GOSAT observations of atmospheric methane. Atmos. Chem. Phys. 21, 4339–4356. https://doi.org/10.5194/acp-21-4339-2021.

McNicol, G., Fluet-Chouinard, E., Ouyang, Z., Knox, S., Zhang, Z., Aalto, T., Bansal, S., Chang, K.-Y., Chen, M., Delwiche, K., Feron, S., Goeckede, M., Liu, J., Malhotra, A., Melton, J.R., Riley, W., Vargas, R., Yuan, K., Ying, Q., Zhu, Q., Alekseychik, P., Aurela, M., Billesbach, D.P., Campbell, D.I., Chen, J., Chu, H., Desai, A.R., Euskirchen, E., Goodrich, J., Griffis, T., Helbig, M., Hirano, T., Iwata, H., Jurasinski, G., King, J., Koebsch, F., Kolka, R., Krauss, K., Lohila, A., Mammarella, I., Nilson, M., Noormets, A., Oechel, W., Peichl, M., Sachs, T., Sakabe, A., Schulze, C., Sonnentag, O., Sullivan, R.C., Tuittila, E.-S., Ueyama, M., Vesala, T., Ward, E., Wille, C., Wong, G.X., Zona, D., Windham-Myers, L., Poulter, B., Jackson, R.B., 2023. Upscaling wetland methane emissions from the FLUXNET-CH4 Eddy Covariance Network (UpCH4 v1.0): model development, Network Assessment, and Budget Comparison. AGU Advances 4, e2023AV000956. https://doi.org/10.1029/2023AV000956.

Melton, J.R., Wania, R., Hodson, E.L., Poulter, B., Ringeval, B., Spahni, R., Bohn, T., Avis, C.A., Beerling, D.J., Chen, G., Eliseev, A.V., Denisov, S.N., Hopcroft, P.O., Lettenmaier, D.P., Riley, W.J., Singarayer, J.S., Subin, Z.M., Tian, H., Zürcher, S., Brovkin, V., van Bodegom, P.M., Kleinen, T., Yu, Z.C., Kaplan, J.O., 2013. Present state of global wetland extent and wetland methane modelling: conclusions from a model inter-comparison project (WETCHIMP). Biogeosciences 10, 753–788. https://doi.org/10.5194/bg-10-753-2013.

Mitra, B., Minick, K., Miao, G., Domec, J.-C., Prajapati, P., McNulty, S.G., Sun, G., King, J. S., Noormets, A., 2020. Spectral evidence for substrate availability rather than environmental control of methane emissions from a coastal forested wetland. Agric. For. Meteorol. 291, 108062. https://doi.org/10.1016/j.agrformet.2020.108062.

Moore, T.R., Dalva, M., 1993. The influence of temperature and water table position on carbon dioxide and methane emissions from laboratory columns of peatland soils. J. Soil Sci. 44, 651–664. https://doi.org/10.1111/j.1365-2389.1993.tb02330.x.

Oh, Y., Zhuang, Q., Liu, L., Welp, L.R., Lau, M.C.Y., Onstott, T.C., Medvigy, D., Bruhwiler, L., Dlugokencky, E.J., Hugelius, G., D'Imperio, L., Elberling, B., 2020. Reduced net methane emissions due to microbial methane oxidation in a warmer Arctic. Nat. Clim. Chang. 10, 317–321. https://doi.org/10.1038/s41558-020-0734-z.

Olefeldt, D., Turetsky, M.R., Crill, P.M., McGuire, A.D., 2013. Environmental and physical controls on northern terrestrial methane emissions across permafrost zones. Glob. Chang Biol. 19, 589–603. https://doi.org/10.1111/gcb.12071.

Pangala, S.R., Enrich-Prast, A., Basso, L.S., Peixoto, R.B., Bastviken, D., Hornibrook, E.R. C., Gatti, L.V., Marotta, H., Calazans, L.S.B., Sakuragui, C.M., Bastos, W.R., Malm, O., Gloor, E., Miller, J.B., Gauci, V., 2017. Large emissions from floodplain trees close the Amazon methane budget. Nature 552, 230–234. https://doi.org/10.1038/nature24639.

Rinne, J., Tuittila, E.-S., Peltola, O., Li, X., Raivonen, M., Alekseychik, P., Haapanala, S., Pihlatie, M., Aurela, M., Mammarella, I., Vesala, T., 2018. Temporal variation of ecosystem scale methane emission from a boreal fen in relation to temperature, water table position, and carbon dioxide fluxes. Global Biogeochem. Cycles 32, 1087–1106. https://doi.org/10.1029/2017GB005747.

Saunois, M., Bousquet, P., Poulter, B., Peregon, A., Ciais, P., Canadell, J.G., Dlugokencky, E.J., Etiope, G., Bastviken, D., Houweling, S., Janssens-Maenhout, G.,

Tubiello, F.N., Castaldi, S., Jackson, R.B., Alexe, M., Arora, V.K., Beerling, D.J., Bergamaschi, P., Blake, D.R., Brailsford, G., Bruhwiler, L., Crevoisier, C., Crill, P., Covey, K., Frankenberg, C., Gedney, N., Höglund-Isaksson, L., Ishizawa, M., Ito, A., Joos, F., Kim, H.-S., Kleinen, T., Krummel, P., Lamarque, J.-F., Langenfelds, R., Locatelli, R., Machida, T., Maksyutov, S., Melton, J.R., Morino, I., Naik, V., O'Doherty, S., Parmentier, F.-J.W., Patra, P.K., Peng, C., Peng, S., Peters, G.P., Pison, I., Prinn, R., Ramonet, M., Riley, W.J., Saito, M., Santini, M., Schroeder, R., Simpson, I.J., Spahni, R., Takizawa, A., Thornton, B.F., Tian, H., Tohjima, Y., Viovy, N., Voulgarakis, A., Weiss, R., Wilton, D.J., Wiltshire, A., Worthy, D., Wunch, D., Xu, X., Yoshida, Y., Zhang, B., Zhang, Z., Zhu, Q., 2017. Variability and quasi-decadal changes in the methane budget over the period 2000-2012. Atmos. Chem. Phys. 17, 11135–11161. https://doi.org/10.5194/acp-17-11135-2017.

Saunois, M., Martinez, A., Poulter, B., Zhang, Z., Raymond, P., Regnier, P., Canadell, J.G., Jackson, R.B., Patra, P.K., Bousquet, P., Ciais, P., Dlugokencky, E.J., Lan, X., Allen, G.H., Bastviken, D., Beerling, D.J., Belikov, D.A., Blake, D.R., Castaldi, S., Crippa, M., Deemer, B.R., Dennison, F., Etiope, G., Gedney, N., Höglund-Isaksson, L., Holgerson, M.A., Hopcroft, P.O., Hugelius, G., Ito, A., Jain, A.K., Janardanan, R., Johnson, M.S., Kleinen, T., Krummel, P., Lauerwald, R., Li, T., Liu, X., McDonald, K.C., Melton, J.R., Mühle, J., Müller, J., Murguia-Flores, F., Niwa, Y., Noce, S., Pan, S., Parker, R.J., Peng, C., Ramonet, M., Riley, W.J., Rocher-Ros, G., Rosentreter, J.A., Sasakawa, M., Segers, A., Smith, S.J., Stanley, E.H., Thanwerdas, J., Tian, H., Tsuruta, A., Tubiello, F.N., Weber, T.S., van der Werf, G., Worthy, D.E., Xi, Y., Yoshida, Y., Zhang, W., Zheng, B., Zhu, Qing, Zhu, Qiuan, Zhuang, Q., 2024. Global methane Budget 2000-2020. Earth System science data discussions 1–147. https://doi.org/10.5194/essd-2024-115.

Saunois, M., Stavert, A.R., Poulter, B., Bousquet, P., Canadell, J.G., Jackson, R.B., Raymond, P.A., Dlugokencky, E.J., Houweling, S., Patra, P.K., Ciais, P., Arora, V.K., Bastviken, D., Bergamaschi, P., Blake, D.R., Brailsford, G., Bruhwiler, L., Carlson, K. M., Carrol, M., Castaldi, S., Chandra, N., Crevoisier, C., Crill, P.M., Covey, K., Curry, C.L., Etiope, G., Frankenberg, C., Gedney, N., Hegglin, M.I., Höglund-Isaksson, L., Hugelius, G., Ishizawa, M., Ito, A., Janssens-Maenhout, G., Jensen, K.M., Joos, F., Kleinen, T., Krummel, P.B., Langenfelds, R.L., Laruelle, G.G., Liu, L., Machida, T., Maksyutov, S., McDonald, K.C., McNorton, J., Miller, P.A., Melton, J.R., Morino, I., Müller, J., Murguia-Flores, F., Naik, V., Niwa, Y., Noce, S., O'Doherty, S., Parker, R.J., Peng, C., Peng, S., Peters, G.P., Prigent, C., Prinn, R., Ramonet, M., Regnier, P., Riley, W.J., Rosentreter, J.A., Segers, A., Simpson, I.J., Shi, H., Smith, S. J., Steele, L.P., Thornton, B.F., Tian, H., Tohjima, Y., Tubiello, F.N., Tsuruta, A., Viovy, N., Voulgarakis, A., Weber, T.S., van Weele, M., van der Werf, G.R., Weiss, R. F., Worthy, D., Wunch, D., Yin, Y., Yoshida, Y., Zhang, W., Zhang, Z., Zhao, Y., Zheng, B., Zhu, Qing, Zhu, Qiuan, Zhuang, Q., 2020. The Global methane Budget 2000-2017. Earth System Science Data 12, 1561–1623. https://doi.org/10.5194/essd-12-1561-2020.

Spahni, R., Wania, R., Neef, L., van Weele, M., Pison, I., Bousquet, P., Frankenberg, C., Foster, P.N., Joos, F., Prentice, I.C., van Velthoven, P., 2011. Constraining global methane emissions and uptake by ecosystems. Biogeosciences 8, 1643–1665. https://doi.org/10.5194/bg-8-1643-2011.

Stocker, T.F., 2013. Climate change 2013: the physical science basis : summary for policymakers, a report of Working Group I of the IPCC, technical summary, a report accepted by Working Group I of the IPCC but not approved in detail and frequently asked questions : part of the Working Group I contribution to the fifth assessment report of the Intergovernmental Panel on Climate Change. Intergovernmental Panel on Climate Change.

Tang, J., Riley, W.J., 2015. Weaker soil carbon–climate feedbacks resulting from microbial and abiotic interactions. Nature Clim Change 5, 56–60. https://doi.org/10.1038/nclimate2438.

Tang, J., Zhuang, Q., 2009. A global sensitivity analysis and bayesian inference framework for improving the parameter estimation and prediction of a process-based Terrestrial ecosystem Model. J. Geophys. Res.: Atmos. 114. https://doi.org/10.1029/2009JD011724.

Tian, H., Chen, G., Lu, C., Xu, X., Ren, W., Zhang, B., Banger, K., Tao, B., Pan, S., Liu, M., Zhang, C., Bruhwiler, L., Wofsy, S., 2015. Global methane and nitrous oxide emissions from terrestrial ecosystems due to multiple environmental changes. Ecosyst. Health Sustain 1, 1–20. https://doi.org/10.1890/EHS14-0015.1.

Tian, H., Xu, X., Liu, M., Ren, W., Zhang, C., Chen, G., Lu, C., 2010. Spatial and temporal patterns of CH_4 and N_2O fluxes in terrestrial ecosystems of North America during 1979-2008: application of a global biogeochemistry model. Biogeosciences 7, 2673–2694. https://doi.org/10.5194/bg-7-2673-2010.

Updegraff, K., Bridgham, S.D., Pastor, J., Weishampel, P., 1998. Hysteresis in the temperature response of carbon dioxide and methane production in peat soils. Biogeochemistry 43, 253–272. https://doi.org/10.1023/A:1006097808262.

Updegraff, K., Pastor, J., Bridgham, S.D., Johnston, C.A., 1995. Environmental and substrate controls over carbon and nitrogen mineralization in Northern wetlands. Ecol. Appl. 5, 151–163. https://doi.org/10.2307/1942060.

Valentine, D.W., Holland, E.A., Schimel, D.S., 1994. Ecosystem and physiological controls over methane production in northern wetlands. J. Geophys. Res.: Atmos. 99, 1563–1571. https://doi.org/10.1029/93JD00391.

Van Vuuren, D.P., Edmonds, J., Kainuma, M., Riahi, K., Thomson, A., Hibbard, K., Hurtt, G.C., Kram, T., Krey, V., Lamarque, J.-F., Masui, T., Meinshausen, M., Nakicenovic, N., Smith, S.J., Rose, S.K., 2011. The representative concentration pathways: an overview. Clim. Change 109, 5–31. https://doi.org/10.1007/s10584-011-0148-z.

Wang, Y., Yuan, Fengming, Yuan, Fenghui, Gu, B., Hahn, M.S., Torn, M.S., Ricciuto, D. M., Kumar, J., He, L., Zona, D., Lipson, D.A., Wagner, R., Oechel, W.C., Wullschleger, S.D., Thornton, P.E., Xu, X., 2019. Mechanistic modeling of microtopographic impacts on CO2 and CH4 fluxes in an Alaskan Tundra ecosystem using the CLM-microbe model. J. Adv. Model. Earth Syst. 11, 4288–4304. https://doi.org/10.1029/2019MS001771.

Wania, R., Ross, I., Prentice, I.C., 2010. Implementation and evaluation of a new methane model within a dynamic global vegetation model. LPJ-WHyMe v1.3.1. Geoscientific Model Dev. 3, 565–584. https://doi.org/10.5194/gmd-3-565-2010.

Wania, R., Ross, I., Prentice, I.C., 2009. Integrating peatlands and permafrost into a dynamic global vegetation model: 1. Evaluation and sensitivity of physical land surface processes. Global Biogeochem. Cycles 23. https://doi.org/10.1029/2008GB003412.

Xu, X., Elias, D.A., Graham, D.E., Phelps, T.J., Carroll, S.L., Wullschleger, S.D., Thornton, P.E., 2015. A microbial functional group-based module for simulating methane production and consumption: application to an incubated permafrost soil. J. Geophys. Res.: Biogeosci. 120, 1315–1333. https://doi.org/10.1002/2015JG002935.

Xu, X., Yuan, F., Hanson, P.J., Wullschleger, S.D., Thornton, P.E., Riley, W.J., Song, X., Graham, D.E., Song, C., Tian, H., 2016. Reviews and syntheses: four decades of modeling methane cycling in terrestrial ecosystems. Biogeosciences 13, 3735–3755. https://doi.org/10.5194/bg-13-3735-2016.

Yavitt, J.B., Lang, G.E., Wieder, R.K., 1987. Control of carbon mineralization to CH4 and CO2 in anaerobic,Sphagnum-derived peat from Big Run Bog, West Virginia. Biogeochemistry 4, 141–157. https://doi.org/10.1007/BF02180152.

Yuan, K., Zhu, Q., Li, F., Riley, W.J., Torn, M., Chu, H., McNicol, G., Chen, M., Knox, S., Delwiche, K., Wu, H., Baldocchi, D., Ma, H., Desai, A.R., Chen, J., Sachs, T., Ueyama, M., Sonnentag, O., Helbig, M., Tuittila, E.-S., Jurasinski, G., Koebsch, F., Campbell, D., Schmid, H.P., Lohila, A., Goeckede, M., Nilsson, M.B., Friborg, T., Jansen, J., Zona, D., Euskirchen, E., Ward, E.J., Bohrer, G., Jin, Z., Liu, L., Iwata, H., Goodrich, J., Jackson, R., 2022. Causality guided machine learning model on wetland CH4 emissions across global wetlands. Agric. Forest Meteorol. 324, 109115. https://doi.org/10.1016/j.agrformet.2022.109115.

Yvon-Durocher, G., Allen, A.P., Bastviken, D., Conrad, R., Gudasz, C., St-Pierre, A., Thanh-Duc, N., del Giorgio, P.A., 2014. Methane fluxes show consistent temperature dependence across microbial to ecosystem scales. Nature 507, 488–491. https://doi.org/10.1038/nature13164.

Zhang, Z., Fluet-Chouinard, E., Jensen, K., McDonald, K., Hugelius, G., Gumbricht, T., Carroll, M., Prigent, C., Bartsch, A., Poulter, B., 2021. Development of the global dataset of Wetland Area and Dynamics for Methane modeling (WAD2M). Earth System Sci. Data 13, 2001–2023. https://doi.org/10.5194/essd-13-2001-2021.

Zhuang, Q., Melillo, J.M., Kicklighter, D.W., Prinn, R.G., McGuire, A.D., Steudler, P.A., Felzer, B.S., Hu, S., 2004. Methane fluxes between terrestrial ecosystems and the atmosphere at northern high latitudes during the past century: a retrospective analysis with a process-based biogeochemistry model. Global Biogeochem. Cycles 18. https://doi.org/10.1029/2004GB002239.